





Uranium-mercury complex antiferromagnet: $\text{UHg}_{6.4}$ Yu. Prots , M. Krnel , M. Schmidt, Yu. Grin , and E. Svanidze **Max-Planck-Institut für Chemische Physik fester Stoffe, Nöthnitzer Straße 40, Dresden 01187, Germany*

(Received 31 March 2022; revised 8 July 2022; accepted 22 August 2022; published 31 August 2022)

Crystallographically complex compounds containing $4f$ and $5f$ electrons often have peculiar chemical and physical properties. In this work we present discovery and characterization of a new material $\text{UHg}_{6.4}$, located at the border to complex intermetallics. This material crystallizes in the $\text{LaHg}_{6.4}$ structure type, which can be represented by La/U-centered polyhedra with coordination numbers of 13 and 14. Much like the $\text{LaHg}_{6.4}$ analog, $\text{UHg}_{6.4}$ shows strong crystallographic disorder, in particular for Hg atoms in the channels along [001]. The $\text{UHg}_{6.4}$ compound orders antiferromagnetically below $T_{N1} = 35.5 \pm 1$ K and displays another transition at $T_{N2} = 47.3 \pm 1$ K, which is likely also antiferromagnetic. Both transitions are only slightly affected by magnetic field. Given high air sensitivity of $\text{UHg}_{6.4}$, an exceptional experimental environment for sample synthesis and characterization was necessary in order to comprehensively describe the chemical and physical properties of this system.

DOI: [10.1103/PhysRevB.106.L060412](https://doi.org/10.1103/PhysRevB.106.L060412)

I. INTRODUCTION

Materials which contain elements from the bottom of the periodic table often exhibits interesting chemical and physical properties, which are deeply interrelated. The role of crystallographic disorder—either intrinsic or induced—is not yet fully understood [1–8]. In particular, heavy-fermion materials seem to be strongly influenced by the minute changes in their crystalline arrangement [8–15]. This motivates design and discovery of new heavy-fermion systems. In the previous work [16] we have shown that crystallographically complex materials offer much promise when it comes to the targeted discovery of new heavy-fermion compounds. Our empirical approach relied on the fulfillment of three parameters, which could perhaps be beneficial for the enhancement of the effective electron mass in uranium-based materials. By looking at compounds that have a coordination number above 12, uranium mass percentage under 40%, and overall shortest uranium interatomic distance above 3 Å, we were able to correctly identify a new heavy-fermion $\text{U}_{23}\text{Hg}_{88}$ [16]. This compound orders antiferromagnetically below $T_N = 2.2$ K and displays a very large effective electron mass enhancement, as evident from $\gamma_n = 630$ mJ mol⁻¹ U K⁻² [16].

Motivated by the success of this approach, we have used it to identify a new heavy-fermion candidate $\text{UHg}_{6.4}$. The crystal structure of this material fulfills the above criteria, moreover, it is located on the border between crystallographically

simple and complex intermetallic compounds, see Fig. 1. While UHg_2 and UHg_3 host 3 and 8 atoms per unit cell, respectively, the $\text{UHg}_{6.4}$ and $\text{U}_{23}\text{Hg}_{88}$ systems have 59 and 444 atoms per unit cell, respectively. However, a comprehensive characterization of single crystalline $\text{UHg}_{6.4}$ revealed that this material likely does not exhibit an enhanced effective electron mass. $\text{UHg}_{6.4}$ orders antiferromagnetically below $T_{N1} = 35.5 \pm 1$ K with another transition observed at $T_{N2} = 47.3 \pm 1$ K. Both transitions are only slightly affected by application of the magnetic field.

II. MATERIALS AND METHODS

When it comes to mercury-based materials, much care must be taken during their synthesis, handling, and characterization—from toxicity concerns to their high chemical reactivity—these systems pose several experimental challenges [16–18]. The complexity of work on mercury-based materials is reflected in a low number of reported systems. For example, among mercury-actinide binary compounds, only three U-Hg [16,19–23], four Th-Hg [24–27], and one Pu-Hg [28] system have been found to exist so far.

All sample preparation and handling was performed in the specialized laboratory, equipped with an Ar-filled glove box system [MBraun, $p(\text{H}_2\text{O}/\text{O}_2) < 0.1$ ppm] [29]. Single crystals of $\text{UHg}_{6.4}$ were synthesized from U powder (prepared from sheet, Goodfellow, 99.98%) and Hg (ChemPur, 99.999%) using self-flux method. The U powder was prepared via repeated hydrogenation/dehydrogenation cycles. The U powder and Hg droplets, mixed in the 5:95 ratio, were sealed in Ta tubes (volume of ≈ 2 cm³ for a sample mass of ≈ 1 g) under Ar atmosphere. The sealed Ta tubes were heated to 500°C, and then slowly cooled to room temperature over a period of 10 days. Excess Hg flux was decanted at room temperature via centrifugation. Some mercury could not be

*Corresponding author: svanidze@cpfs.mpg.de

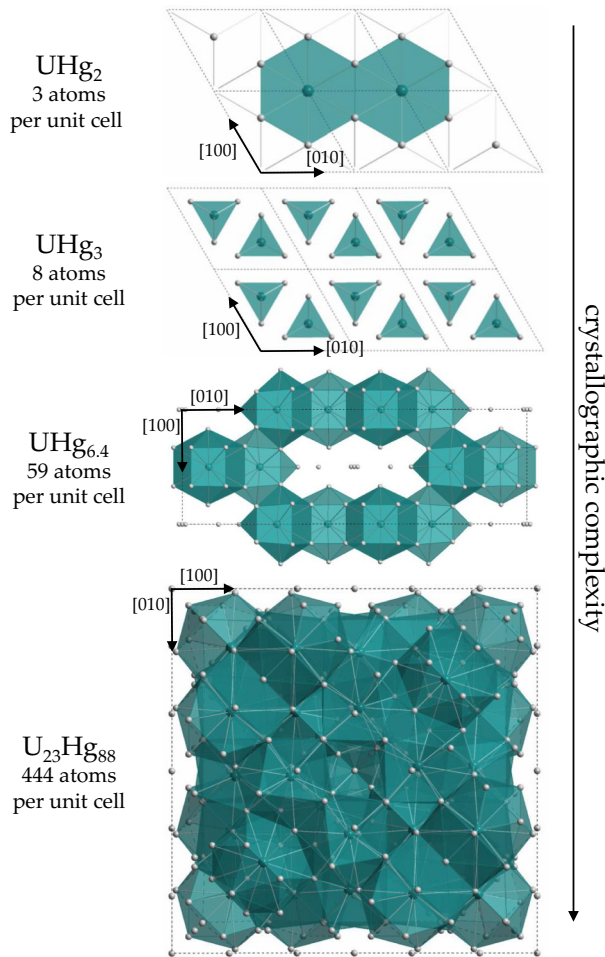


FIG. 1. Four uranium-mercury compounds arranged according to their crystallographic complexity from the simplest (smallest number of atoms per unit cell, top) to the most complex (largest number of atoms per unit cell, bottom). Note that while six unit cells are shown for UHg_2 and UHg_3 , only one is shown for $\text{UHg}_{6.4}$ and $\text{U}_{23}\text{Hg}_{88}$.

completely removed from the surface of the crystals. The resultant crystals had silver luster and needlelike morphology, with some examples shown in Fig. 2. Similar to the other U-Hg binary compounds [16,20,21,30–32], the $\text{UHg}_{6.4}$ phase exhibits extreme air and moisture sensitivity, resulting in immediate decomposition even after short exposure to air. Additionally, the $\text{UHg}_{6.4}$ crystals are rather fragile, breaking easily when touched by tweezers. Four batches of $\text{UHg}_{6.4}$ have been prepared for the current study in the same exact way. However, it appears some variation between crystals exists, as shown in Fig. 5(a). This difference can be due to the variation of the Hg concentration, as a result of crystallographic disorder (see Fig. 3, Sec. III A, and Ref. [33]), as well as small amount of elemental Hg that cannot be removed from the surface and the interior of the crystals.

Powder x-ray diffraction was performed on a Huber G670 Image plate Guinier camera with a Ge-monochromator ($\text{Cu } K\alpha_1$, $\lambda = 1.54056 \text{ \AA}$). Phase identification was done using the WinXPow software [34]. The lattice parameters were deter-

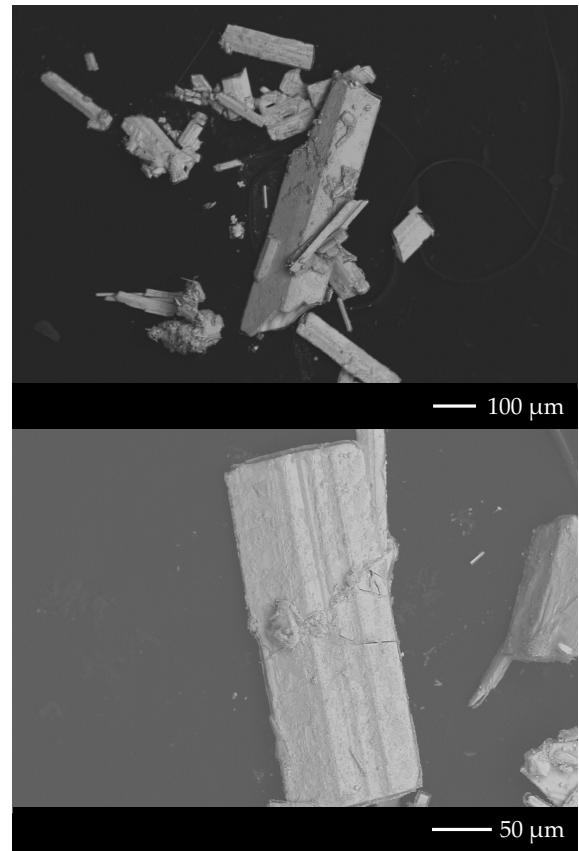


FIG. 2. Backscatter electron micrographs of $\text{UHg}_{6.4}$ single crystals. Minute exposure to air results in an immediate degradation of the sample, as evidenced by the rough surface of the single crystals and microscopic droplets of mercury, appearing on their surface. Cracks are consistent with mechanical fragility.

mined by a least-squares refinement using the peak positions, extracted by profile fitting. Single crystal diffraction data were collected on small single crystals ($\approx 50 \mu\text{m}$ in size) using a Rigaku AFC7 diffractometer, equipped with a Saturn 724+ CCD detector and a Mo $K\alpha$ radiation source ($\lambda = 0.71073 \text{ \AA}$). The WinCSD software [35] was used for crystallographic analysis (see Tables I and II).

Differential thermal analysis (DTA) was performed on a Netzsch DTA 404 PC in the range from 30 to 500 °C, in a sealed quartz ampoule in a steady Ar flow with a heating/cooling rate of 5 K min^{-1} . The ampoule was sealed under vacuum, while being cooled in LN_2 . An empty quartz ampoule of the same size was used for background subtraction. The resultant data are shown in Fig. S1 [36], the onset of the decomposition around 460 °C of $\text{UHg}_{6.4}$ is marked by vertical arrows and is comparable to other U-Hg binaries [16,21,31,37].

The magnetic properties were studied using a Quantum Design (QD) Magnetic Property Measurement System for the temperature range from $T = 1.8 \text{ K}$ to $T = 300 \text{ K}$ and for applied magnetic fields up to $H = 7 \text{ T}$. The inverse magnetic susceptibility data were fit to the Curie-Weiss law, after a temperature-independent contribution has been subtracted ($0.5 \times 10^{-3} \leq \chi_0 \leq 1.3 \times 10^{-3} \text{ emu mol}_{\text{F.U.}}^{-1}$). The

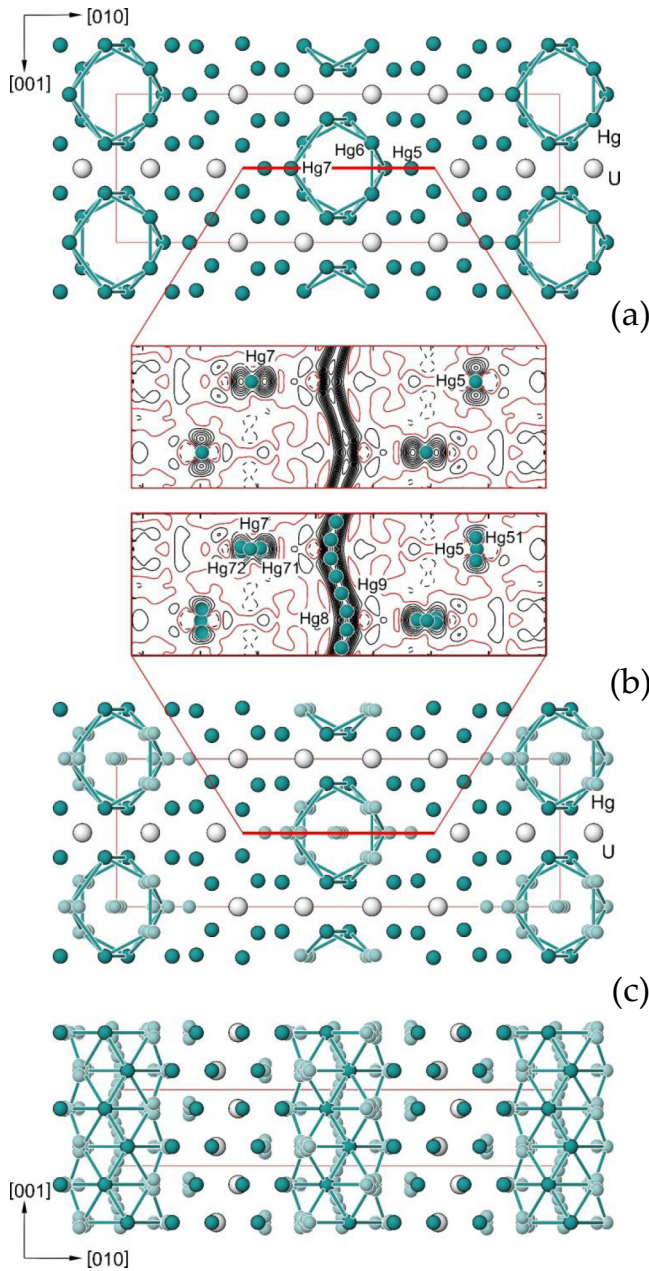


FIG. 3. Crystal structure determination of $\text{UHg}_{6.4}$: (a) Upper panel: partial crystal structure involving the U1-U2 and Hg1-Hg7 positions (see Table II). (a) Lower panel: Distribution of the difference electron density in the part of (200) plane marked in red in the upper panel together with the positions Hg5 and Hg7. (b) Upper panel: Distribution of the difference electron density in the part of (200) plane marked in red in the lower panel and the projection of the crystal structure involving the split positions around Hg5 and Hg7, as well as the split positions Hg8 and Hg9 within the channel. (c) Projection of the structure along [010] visualizing the channels running along [001].

specific heat data were collected on a QD Physical Property Measurement System from $T = 0.4$ K to $T = 100$ K for magnetic fields up to $H = 9$ T. The values of the ordering temperature were taken from the peak value in the (i) dMT/dT [Fig. 7(a)] and (ii) dC_p/dT [Fig. 7(b)]. Given high air sensitiv-

TABLE I. Crystallographic data for $\text{UHg}_{6.4}$ ($\text{LaHg}_{6.4}$ structure type).

Crystal system	Orthorhombic
Space group	$Cmcm$ (No. 63)
Formula units per cell	$Z = 8$
Unit cell parameters	
a	9.629(2) Å
b	28.779(7) Å
c	4.943(1) Å
Unit cell volume, V	1370.5(5) Å ³
Calculated density	14.8 g cm ⁻³
Crystal form	platelike
Crystal size	20 × 90 × 150 μm ³
Diffraction system	RIGAKU AFC7
Detector	Saturn 724+ CCD
Radiation type, λ	Mo $K\alpha$, 0.71073 Å
Scan; step/deg; $N(\text{images})$	ϕ , 0.6, 600
Maximal 2θ	64°
Range in h, k, l	$-13 \leq h \leq 14$, $-42 \leq k \leq 34$, $-3 \leq l \leq 7$
Absorption correction	multiscan + numerical
$N(hkl)$ measured	4878
$N(hkl)$ unique	1362
$N(hkl)$ observed	1027
R_{int}	0.049
Refined parameters	71
Residual peaks	$-1.08/1.45e^{-3}$
R_F, R_w	0.049, 0.049

ity, coupled with mechanical fragility of the $\text{UHg}_{6.4}$ crystals, it was not possible to carry out any resistivity measurements.

III. RESULTS AND DISCUSSION

A. Crystal structure

Mercury-based compounds and amalgams often host peculiar crystallographic environments [16,23,38–47] and display unusual bonding features [44,48–54]. As a result, some of these materials show peculiar superconducting [33,52,55–68] or magnetic [16,32,69–73] ground states.

The newly discovered $\text{UHg}_{6.4}$ is the Hg-richest phase in the U-Hg system, crystallizing in the $\text{LaHg}_{6.4}$ structure type. While the first report about the existence of the $\text{LaHg}_{6.4}$ structure type suggested orthorhombic crystal structure and correctly identified lattice parameters in 1976 [74], the complete structural characterization of $\text{LaHg}_{6.4}$ has been missing for nearly 50 years [33]. This can be explained by the experiential difficulty of Hg-based materials—in addition to high x-ray absorption, the $\text{UHg}_{6.4}$ compound is highly air sensitive, decomposing immediately even after minute exposure to air. In our recent work [33] we were able to comprehensively describe the structural and physical properties of $\text{LaHg}_{6.4}$. This compound crystallizes in the $Cmcm$ space group [$a = 9.779(2)$ Å, $b = 28.891(4)$ Å, and $c = 5.0012(8)$ Å] and enters superconducting state below $T_c = 2.4$ K. Strong disorder was found to exist in the structure of $\text{LaHg}_{6.4}$, with partially occupied chains of mercury propagating along the [001] direction [33].

TABLE II. Atomic coordinates, Wyckoff sites, and isotropic displacement parameters (\AA^2) for $\text{UHg}_{6.4}$, obtained from the single crystal x-ray refinement.

Atom	Wyckoff site	x/a	y/b	z/c	$B_{\text{iso/eq}}$	Occupancy
U1	4c	1/2	0.07663(3)	3/4	0.89(2)	1.0
U2	4c	1/2	0.22532(3)	1/4	1.03(2)	1.0
Hg1	8g	0.32359(9)	0.18043(3)	3/4	1.60(2)	1.0
Hg2	8g	0.33352(9)	0.12606(2)	1/4	1.35(2)	1.0
Hg3	8g	0.33343(9)	0.02528(2)	1/4	1.45(2)	1.0
Hg4	8g	0.15609(9)	0.21553(3)	1/4	1.55(2)	1.0
Hg5	4c	0	0.16555(4)	3/4	1.41	0.77(1)
Hg51	8f	0	0.1645(2)	0.668(1)	1.33	0.115
Hg6	8g	0.1718(2)	0.07637(4)	3/4	1.30	0.597(3)
Hg61	16h	0.1686(4)	0.07092(9)	0.7019(6)	1.30	0.151(3)
Hg62	16h	0.172(2)	0.0839(4)	0.682(2)	1.30	0.038(3)
Hg63	8g	0.165(2)	0.0641(5)	3/4	1.30	0.053(2)
Hg7	4c	0	0.89423(7)	1/4	2.01(4)	0.584(10)
Hg71	8f	0	0.0941(2)	0.257(6)	2.439	0.12(1)
Hg72	8f	0	0.1166(3)	0.267(3)	1.717	0.08(1)
Hg8	8f	1/2	0.5096(1)	0.3153(7)	1.73(15)	0.187(6)
Hg9	8f	1/2	0.5032(2)	0.4404(7)	1.7(2)	0.177(6)

The crystal structure of $\text{UHg}_{6.4}$ was determined from the x-ray single crystal diffraction data. The crystallographic information is presented in Table I. Application of a charge-flip technique allows us to determine the ordered part of the crystal structure including the U1–U2 and Hg1–Hg7 positions [Fig. 3(a), upper panel]. The relatively low R value of approximately 0.076 hints toward a reasonable model. A striking feature of this model is the clearly enhanced values of the atomic displacement parameters for the Hg5–Hg7 positions. Calculation of the different electron density at this stage revealed several additional maxima around Hg5, Hg7 [Fig. 3(a), lower panel], and Hg6 position, indicating strong disorder in the vicinity of these sites. Furthermore, the quasicontinuous distribution was observed around $00z$ and $\frac{1}{2}\frac{1}{2}z$ axes. In order to describe this distribution, two split sites were used around Hg5 position, three for Hg7, and four for Hg6 positions, respectively. Furthermore, two split sites, Hg8 and Hg9, were necessary for describing the difference density in the channels $00z$ and $\frac{1}{2}\frac{1}{2}z$ [Fig. 3(b), upper panel]. The whole disorder in the crystal structure [Fig. 3(b), lower panel; Fig. 3(c)] is obviously caused by the incommensurability of the basic structure and the Hg substructure within the channels. Depending on the local positions of the channel atoms, the channel wall breathes and adjusts its local arrangement to the channel fillers. This leads also to the noninteger composition $\text{UHg}_{6.4}$ with ~ 59 atoms in the unit cell.

The crystallographic disorder in $\text{UHg}_{6.4}$ is similar to the recently discovered in the lanthanum analog [33]. In $\text{LaHg}_{6.4}$, the disorder around the Hg5 and Hg6 positions was indicated only by strong anisotropy of atomic displacement, for the Hg7 position, four split sites were necessary, and three sites were detected in the channels. The stoichiometry of both uranium- and lanthanum-containing materials is 1:6.4. The majority of the Hg–Hg distances vary between $2.41 \leq d_{(\text{Hg}-\text{Hg})} \leq 3.92$ \AA , similar to what is observed in elemental Hg ($d_{(\text{Hg}-\text{Hg})} = 2.99\text{--}3.46$ \AA).

Interestingly, the uranium-uranium shortest distance $d_{(\text{U}-\text{U})} = 4.94$ \AA is rather large (for example, in elemental uranium $d_{(\text{U}-\text{U})} = 2.75\text{--}3.43$ \AA). According to the Hill limit [75], such large separation of the uranium atoms is likely to yield a magnetic ground state, as shown in Sec. III B.

For the uranium atoms, two crystallographic positions exist. As summarized in Fig. 4, U1 is coordinated by 14 Hg atoms in the form of bicapped hexagonal prisms (green),

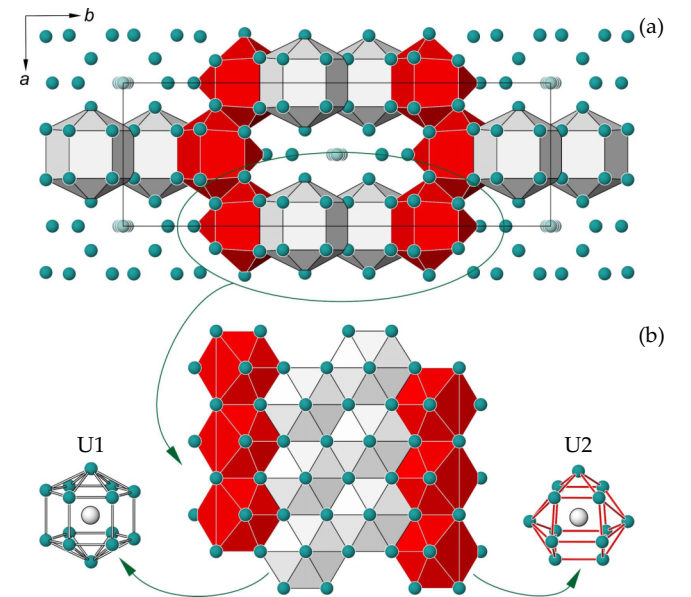


FIG. 4. Crystal structure of $\text{UHg}_{6.4}$: (a) The view of the crystal structure in the polyhedral representation along the $[001]$ direction. (b) Whole structure represented by an arrangement of U-centered bicapped hexagonal prism (U1, gray, left) and modified cuboctahedra, where one apex is replaced by two Hg atoms (U2, red, right).

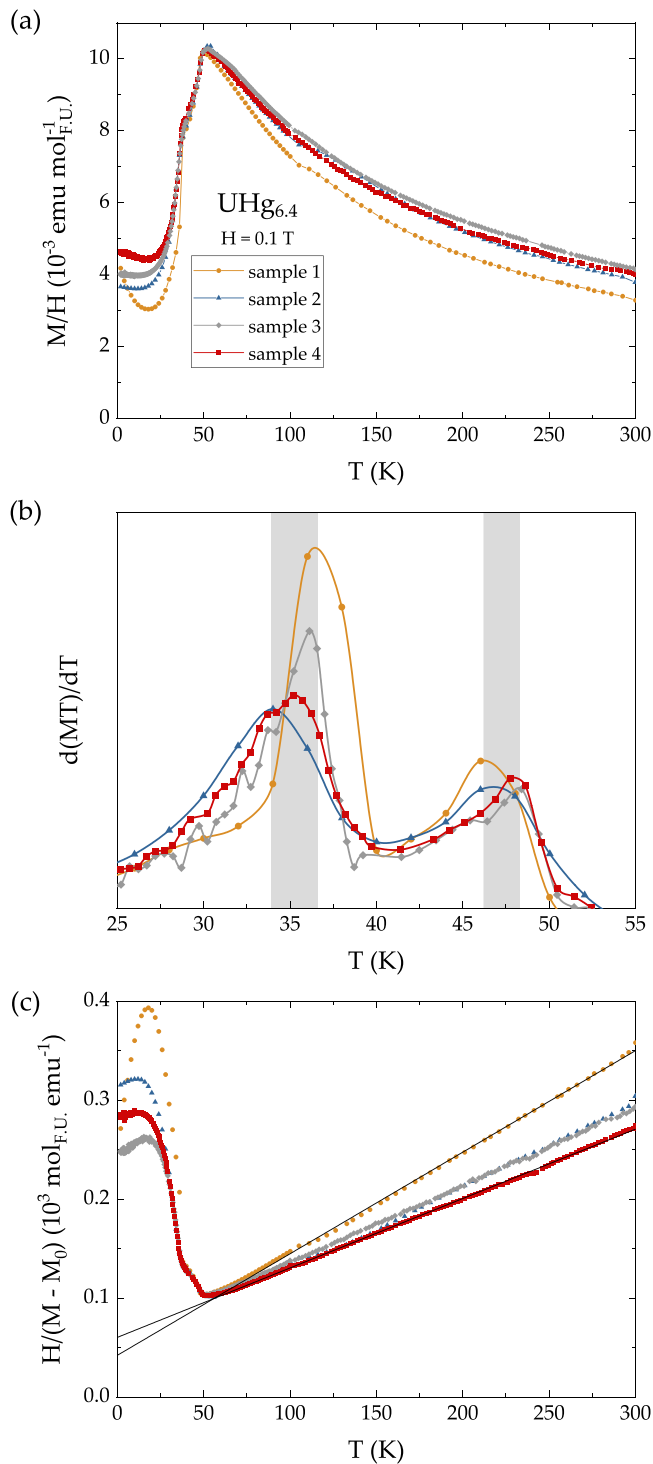


FIG. 5. Magnetic properties of $\text{UHg}_{6.4}$: (a) Magnetic susceptibility as a function of temperature in $H = 0.1$ T for four $\text{UHg}_{6.4}$ samples. All samples exhibit two consecutive magnetic transitions—one at $T_{N1} = 35.5 \pm 1$ K and another at $T_{N2} = 47.3 \pm 1$ K. (b) Inverse magnetic susceptibility of $\text{UHg}_{6.4}$ for four different samples.

while U2 is coordinated by 13 Hg atoms (red). The coordination of U2 can be described as a modified cuboctahedron, where one apex is replaced by two Hg atoms. In comparison,

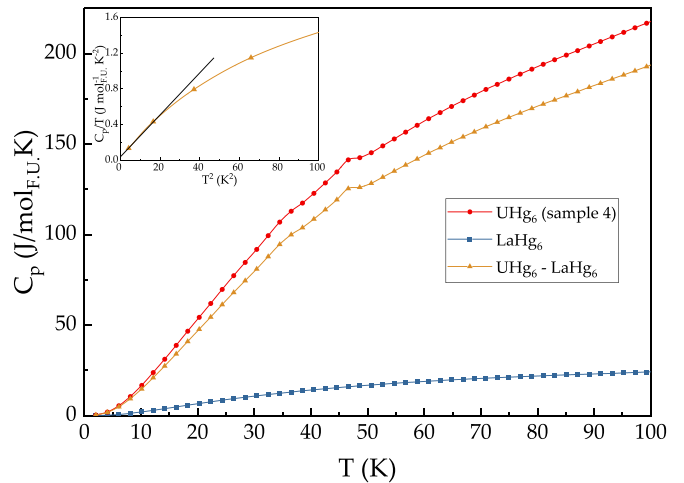


FIG. 6. Temperature-dependent specific heat data of $\text{UHg}_{6.4}$: as-measured data (red) and the data after the $\text{LaHg}_{6.4}$ nonmagnetic analog has been subtracted (orange). Inset shows low-temperature region of the C_p/T vs T^2 plot.

in $\text{U}_{23}\text{Hg}_{88}$, uranium atoms have regular cuboctahedra as coordination polyhedra [16].

B. Magnetic properties

Among U-Hg compounds, physical and chemical properties of UHg_2 [19–21], UHg_3 [20–22], and $\text{U}_{23}\text{Hg}_{88}$ [16,23] have been studied in detail. Interestingly, all three U-Hg compounds order antiferromagnetically below $T_{N1} = 80$ K (UHg_2 [16,76,77]), $T_{N1} = 15$ K (UHg_3 [16,32,77,78]), and $T_{N1} = 2.2$ K ($\text{U}_{23}\text{Hg}_{88}$ [16]).

Temperature-dependent magnetic susceptibility and specific heat of $\text{UHg}_{6.4}$ are shown in Figs. 5 and 6, respectively. It is important to note that some variation exists between four batches of the $\text{UHg}_{6.4}$ samples, prepared for the current study. While all four samples exhibit two consecutive magnetic transitions, the shape of the low-temperature region as well as the temperature-independent contribution χ_0 are different. This could arise from the partial occupancy of mercury, as a result of crystallographic disorder observed in the structure (see Fig. 3 and Ref. [33]), as well as a small amount of elemental Hg that cannot be removed from the crystals. From the derivative of magnetization $d(MT)/dT$, shown in Fig. 5(b), the values of the transition temperatures have been extracted $T_{N1} = 35.5 \pm 1$ K and $T_{N2} = 47.3 \pm 1$ K (gray regions). After subtraction of the temperature-independent contribution to the magnetic susceptibility $0.5 \times 10^{-3} \leq \chi_0 \leq 1.3 \times 10^{-3}$ emu mol $_{\text{F.U.}}^{-1}$, the inverse magnetic susceptibility of $\text{UHg}_{6.4}$ was fit to the Curie-Weiss law above $T = 50$ K, see Fig. 5(c). The resultant effective moment is $2.79 \leq \mu_{\text{eff}} \leq 3.38 \mu_B \text{U}^{-1}$. Both sign and magnitude of the Weiss temperature $-24 \text{ K} \leq \theta_W \leq -41 \text{ K}$ are consistent with an antiferromagnetic ordering of $\text{UHg}_{6.4}$ below $T_{N1} = 35.5 \pm 1$ K.

The field-dependent magnetization data of $\text{UHg}_{6.4}$ are consistent with the antiferromagnetic ground state, as summarized in Fig. S2 [36]. For both $T = 1.8$ K and $T = 2$ K isotherms, linear field dependence is observed, with no distinguishable hysteresis. Linear behavior is also seen for

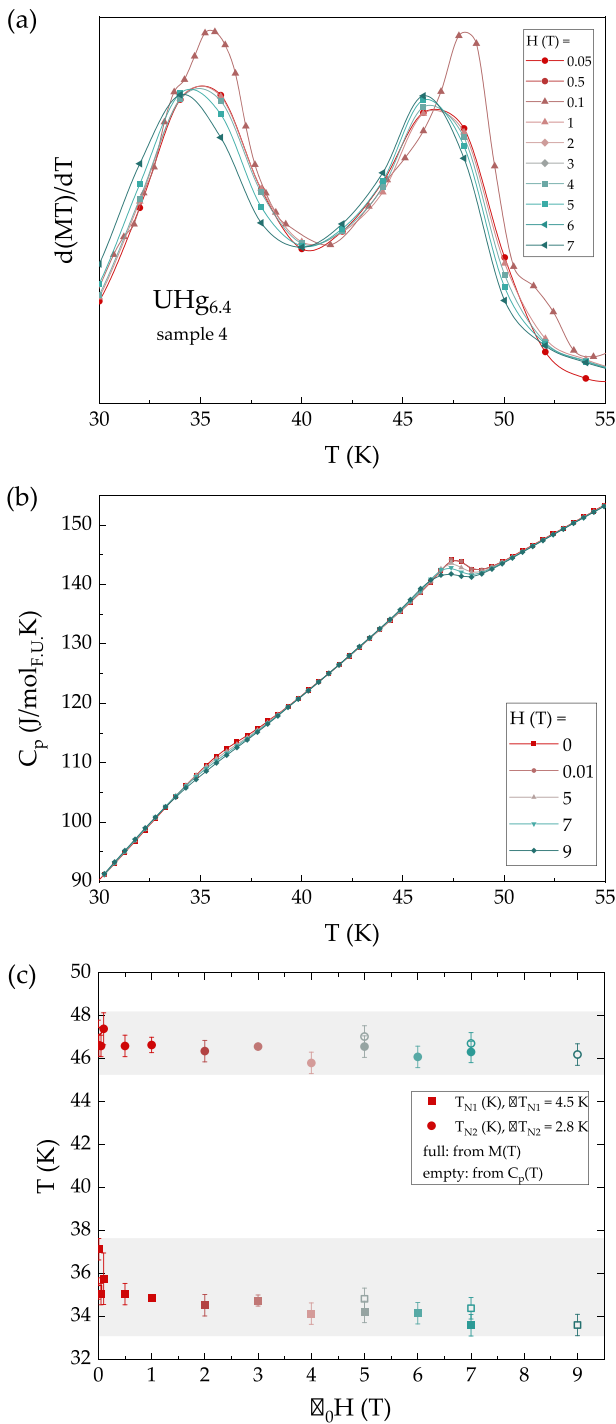


FIG. 7. Evolution of magnetism in $\text{UHg}_{6.4}$ with application of magnetic field: (a) Magnetization and (b) specific heat of $\text{UHg}_{6.4}$ in various magnetic fields. (c) The values of T_{N1} (squares) and T_{N2} (circles), extracted from magnetic [full symbols, (a)] and specific heat [empty symbols, (b)] data.

the magnetic isotherm taken at $T = 40$ K (above T_{N1} but below T_{N2}). Both T_{N1} and T_{N2} transitions are only slightly affected by an applied magnetic field, as shown by the temperature-dependent magnetization [Fig. 7(a)] and specific heat [Fig. 7(b)] data. An H - T phase diagram, presented in Fig. 7(c), reveals a 12% and 6% suppression of T_{N1} and T_{N2} , respectively. Given high ordering temperature of $\text{UHg}_{6.4}$, it was not possible to extract the value of the Sommerfeld coefficient γ from the paramagnetic state. However, low-temperature specific heat data of $\text{UHg}_{6.4}$ (Fig. 6, inset) can be used to provide an upper-limit estimate from (i) an extrapolation of the linear fit ($\gamma_0 = 39$ mJ mol $^{-1}$ U K $^{-2}$) and (ii) the lowest temperature value of $C_p/T = 134$ mJ mol $^{-1}$ U K $^{-2}$. Both of these values are likely an overestimate, given the magnetic contribution to the specific heat. It is therefore likely that the intrinsic value of γ is not enhanced, compared to the free electron scenario.

IV. CONCLUSIONS

In this work we present the discovery and characterization of a new compound—a complex antiferromagnet $\text{UHg}_{6.4}$. It crystallizes in the $\text{LaHg}_{6.4}$ structure type and exhibits strong crystallographic disorder. The material orders antiferromagnetically below $T_{N1} = 35.5 \pm 1$ K with a successive antiferromagnetic transition at $T_{N2} = 47.3 \pm 1$ K. The reduction of both T_{N1} and T_{N2} are rather small even with magnetic fields of up to 9 T. No enhancement of the effective electron mass has been observed in $\text{UHg}_{6.4}$, despite it fulfilling the criteria proposed by our empirical analysis of uranium-based heavy-fermion materials [16]. While the reason behind this deviation remains to be revealed, one possibility is the effect of crystallographic disorder, which is very prominent in the $\text{UHg}_{6.4}$ system. Further analysis of the role of disorder in both heavy-fermion and non-heavy-fermion uranium-based systems can pinpoint the exact relation between the two.

The $\text{UHg}_{6.4}$ compound is located on the border of crystallographic complexity—between simple UHg_2 and UHg_3 on one side and the complex $\text{U}_{23}\text{Hg}_{88}$ on the other side. By looking at the crystallographic complexity across the U-Hg series, the relation between the crystal chemistry and ground state properties is examined. Mercury-based compounds pose several handling difficulties, therefore this work also contributes to the advancement of the synthesis and characterization methods for highly air-sensitive materials.

ACKNOWLEDGMENTS

E.S. is grateful for the support of the Christiane Nüsslein-Volhard-Stiftung. The authors thank U. Burkhardt and M. Brando for fruitful discussions.

[1] M. H. Hamidian, A. R. Schmidt, I. A. Firmo, M. P. Allan, P. Bradley, J. D. Garrett, T. J. Williams, G. M. Luke, Y. Dubi, A. V. Balatsky, and J. C. Davis, How Kondo-holes create intense nanoscale heavy-fermion hybridization disorder, *Proc. Natl. Acad. Sci.* **108**, 18233 (2011).

[2] G. Adrian, H. Adrian, W. Möhle, W. Gerhäuser, M. Lippert, B. Hensel, and H. Niederhofer, Irradiation induced disorder effects in heavy fermion systems, *J. Magn. Magn. Mater.* **76-77**, 642 (1988).

- [3] P. Gegenwart, F. Kromer, M. Lang, G. Sparn, C. Geibel, and F. Steglich, Non-Fermi-Liquid Effects at Ambient Pressure in a Stoichiometric Heavy-Fermion Compound with Very Low Disorder: $\text{CeNi}_{2-z}\text{Ge}_2$, *Phys. Rev. Lett.* **82**, 1293 (1999).
- [4] R. Oishi, Y. Ohmagari, Y. Kusanose, Y. Yamane, K. Umeo, Y. Shimura, T. Onimaru, and T. Takabatake, Heavy-fermion behavior in a honeycomb Kondo lattice CePt_6Al_3 , *J. Phys. Soc. Jpn.* **89**, 104705 (2020).
- [5] P. Swatek and D. Kaczorowski, Heavy fermion behavior in $\text{UT}_2\text{Zn}_{20}$ ($T = \text{Fe, Co, Ru, Rh, Ir}$) compounds, *J. Phys. Soc. Jpn.* **80**, SA106 (2011).
- [6] P. Gegenwart, Q. Si, and F. Steglich, Quantum criticality in heavy-fermion metals, *Nat. Phys.* **4**, 186 (2008).
- [7] F. P. Toldin, J. Figgins, S. Kirchner, and D. K. Morr, Disorder and quasiparticle interference in heavy-fermion materials, *Phys. Rev. B* **88**, 081101(R) (2013).
- [8] M. B. Tang, H. Y. Bai, W. H. Wang, D. Bogdanov, K. Winzer, K. Samwer, and T. Egami, Heavy-fermion behavior in cerium-based metallic glasses, *Phys. Rev. B* **75**, 172201 (2007).
- [9] J. C. Sarrao, C. D. Immer, C. L. Benton, Z. Fisk, and J. Lawrence, Evolution from first-order valence transition to heavy-fermion behavior, *Phys. Rev. B* **54**, 12207 (1996).
- [10] E. G. Moshopoulou, Z. Fisk, J. L. Sarrao, and J. D. Thompson, Crystal growth and intergrowth structure of the new heavy fermion materials CeIrIn_5 and CeRhIn_5 , *J. Solid State Chem.* **158**, 25 (2001).
- [11] J. A. Mydosh, Disorder and frustration in heavy-fermion compounds, *Phys. B: Condens. Matter* **259-261**, 882 (1999).
- [12] J. L. Sarrao, C. L. Benton, Z. Fisk, J. M. Lawrence, D. Mandrus, and J. D. Thompson, $\text{YbIn}_{1-x}\text{Ag}_x\text{Cu}_4$: Crossover from first-order valence transition to heavy Fermion behavior, *Phys. B: Condens. Matter* **223-224**, 366 (1996).
- [13] D. Louca, J. D. Thompson, J. M. Lawrence, R. Movshovich, C. Petrovic, J. L. Sarrao, and G. H. Kwei, Atomic disorder in the heavy fermion superconductor, *Phys. Rev. B* **61**, R14940 (2000).
- [14] W. M. Yuhasz, N. A. Frederick, P. C. Ho, N. P. Butch, B. J. Taylor, T. A. Sayles, M. B. Maple, J. B. Betts, A. H. Lacerda, P. Rogl, and G. Giester, Heavy-fermion behavior, crystalline electric field effects, and weak ferromagnetism in $\text{SmOs}_4\text{Sb}_{12}$, *Phys. Rev. B* **71**, 104402 (2005).
- [15] Z. Hossain, C. Geibel, T. Radu, Y. Tokiwa, F. Weickert, C. Krellner, H. Jeevan, P. Gegenwart, and F. Steglich, Low-temperature properties of the heavy fermion system YbIr_2Si_2 , *Phys. B: Condens. Matter* **378-380**, 74 (2006).
- [16] E. Svanidze, A. Amon, R. Borth, Y. Prots, M. Schmidt, M. Nicklas, A. Leithe-Jasper, and Y. Grin, Empirical way for finding new uranium-based heavy-fermion materials, *Phys. Rev. B* **99**, 220403(R) (2019).
- [17] A. Morawski, A. Paszewin, T. Lada, and H. Marciniak, Mercury superconductors crystal growth under high pressure and high temperature influenced by crucible composition, *IEEE Trans. Appl. Supercond.* **7**, 1903 (1997).
- [18] B. Loret, A. Forget, J. B. Moussy, S. Poissonnet, P. Bonnaillie, G. Collin, P. Thuéry, A. Sacuto, and D. Colson, Crystal growth and characterization of $\text{HgBa}_2\text{Ca}_2\text{Cu}_3\text{O}_{8+\delta}$ superconductors with the highest critical temperature at ambient pressure, *Inorg. Chem.* **56**, 9396 (2017).
- [19] D. H. Ahmann, R. R. Baldwin, and A. S. Wilson, The uranium-mercury system (U.S. Atomic Energy Commission, Division of Technical Information, Washington, DC, 1945).
- [20] R. E. Rundle and A. S. Wilson, The structures of some metal compounds of uranium, *Acta Crystallogr.* **2**, 148 (1949).
- [21] B. R. Frost, The system uranium-mercury, *Vacuum* **4**, 368 (1954).
- [22] R. Ferro, The crystal structures of ThHg_3 , ThIn_3 , ThTl_3 , ThSn_3 and ThPb_3 , *Acta Crystallogr.* **11**, 737 (1958).
- [23] F. Merlo and M. L. Fornasini, Crystal structure of the $\text{R}_{11}\text{Hg}_{45}$ compounds ($\text{R} = \text{La, Ce, Pr, Nd, Sm, Gd, U}$), *J. Less-Common Met.* **64**, 221 (1979).
- [24] R. Domagala, R. Elliott, and W. Rostoker, The system mercury-thorium, *Trans. Metall. Soc. AIME* **212** (1958).
- [25] C. Guminski, The Hg-Th (mercury-thorium) system, *J. Phase Equilib.* **15**, 204 (1994).
- [26] P. Ettmayer, Beitrag zum system quecksilber-thorium, *Monatshefte Chem. Verwandte Teile Anderer Wissenschaften* **96**, 443 (1965).
- [27] A. Palenzona, Th_2Hg : Another representative of the CuAl_2 -type structure, *J. Less-Common Met.* **125**, L5 (1986).
- [28] A. Berndt, A gamma-phase in the plutonium-mercury system, *J. Less-Common Met.* **11**, 216 (1966).
- [29] A. Leithe-Jasper, H. Borrmann, and W. Hönle, Max planck institute for chemical physics of solids, Scientific report (Dresden, 2006).
- [30] F. A. Rough and A. A. Bauer, Constitution of uranium and thorium alloys, Technical Report No. BMI-1300 (Battelle Memorial Inst., Columbus, Ohio, 1958).
- [31] C. Guminski, The Hg-U (mercury-uranium) system, *J. Phase Equilib.* **24**, 461 (2003).
- [32] J. S. Kim and G. R. Stewart, UHg_3 : A heavy-fermion antiferromagnet similar to U_2Zn_{17} and UCd_{11} , *Phys. Rev. B* **89**, 041103(R) (2014).
- [33] Y. Prots, M. Krmel, Y. Grin, and E. Svanidze, Superconductivity in crystallographically disordered $\text{LaHg}_{6.4}$, *Inorganic Chemistry* (to be published) (2022).
- [34] *WinXPow (version 2)* (Darmstadt, STOE and Cie GmbH, 2001).
- [35] L. Akselrud and Y. Grin, WinCSD: Software package for crystallographic calculations (Version 4), *J. Appl. Crystallogr.* **47**, 803 (2014).
- [36] See Supplemental Material at <http://link.aps.org/supplemental/10.1103/PhysRevB.106.L060412> for the differential thermal analysis data, as well as magnetization data for the newly discovered $\text{UHg}_{6.4}$ compound.
- [37] T. S. Lee, P. Chiotti, and J. T. Mason, Phase relations in the uranium-mercury system, *J. Less-Common Met.* **66**, 33 (1979).
- [38] A. Iandelli and R. Ferro, Crystal structure of the compounds LaHg , CeHg , PrHg , and NdHg , *Atti Accad. Naz. Lincei* **8**, 10 (1951).
- [39] A. Iandelli, The structure of some ternary intermetallic compounds of the rare earths, *J. Alloys Compd.* **203**, 137 (1994).
- [40] A. V. Tkachuk and A. Mar, In search of the elusive amalgam SrHg_8 : A mercury-rich intermetallic compound with augmented pentagonal prisms, *Dalton Trans.* **39**, 7132 (2010).
- [41] E. Todorov and S. C. Sevov, Synthesis and structure of the alkali-metal amalgams A_3Hg_{20} ($\text{A} = \text{Rb, Cs}$), K_3Hg_{11} , $\text{Cs}_5\text{Hg}_{19}$, and A_7Hg_{31} ($\text{A} = \text{K, Rb}$), *J. Solid State Chem.* **149**, 419 (2000).

- [42] H. J. Deiseroth and E. Biehl, NaK₂₉Hg₄₈: A contradiction to or an extension of theoretical concepts to rationalize the structures of complex intermetallics?, *J. Solid State Chem.* **147**, 177 (1999).
- [43] E. Biehl and H. J. Deiseroth, Preparation, structural relations, and magnetism of amalgams MHg₁₁ (M: K, Rb, Ba, Sr), *Z. Anorg. Allg. Chem.* **625**, 1073 (1999).
- [44] A. V. Tkachuk and A. Mar, Li₆A₁₇Hg₉ (A = Ca, Sr, Yb): Intermetallic compounds of mercury with a zeolite-like topology of cubic networks, *Chem. Eur. J.* **15**, 10348 (2009).
- [45] J. Sappl, R. Freund, and C. Hoch, Stuck in our teeth? Crystal structure of a new copper amalgam, Cu₃Hg, *Crystals* **7**, 352 (2017).
- [46] F. Tambornino and C. Hoch, The simplest representative of a complex series: The Hg-rich amalgam Yb₁₁Hg₅₄, *Z. Kristallogr. Cryst. Mater.* **232**, 557 (2017).
- [47] A. F. Berndt, The crystal structure of Ce₅Hg₂₁, *J. Less-Common Met.* **13**, 366 (1967).
- [48] F. Tambornino and C. Hoch, The mercury-richest Europium amalgam Eu₁₀Hg₅₅, *Z. Anorg. Allg. Chem.* **641**, 537 (2015).
- [49] C. Hoch and A. Simon, Cs₂Hg₂₇, das quecksilberreichste amalgam ein naher verwandter der Bergman-Phasen, *Z. Anorg. Allg. Chem.* **634**, 853 (2008).
- [50] A. V. Tkachuk and A. Mar, Alkaline-earth metal mercury intermetallics A_{11-x}Hg_{54+x} (A = Ca, Sr), *Inorg. Chem.* **47**, 1313 (2008).
- [51] F. Tambornino and C. Hoch, Bad metal behaviour in the new Hg-rich amalgam KHg₆ with polar metallic bonding, *J. Alloys Compd.* **618**, 299 (2015).
- [52] M. T. Orlando, C. A. Passos, J. L. Passamai, E. F. Medeiros, C. G. Orlando, R. V. Sampaio, H. S. Correa, F. C. De Melo, L. G. Martinez, and J. L. Rossi, Distortion of ReO₆ octahedron in the Hg_{0.82}Re_{0.18}Ba₂Ca₂Cu₃O_{8+d} superconductor, *Physica C* **434**, 53 (2006).
- [53] W. Klein, R. K. Kremer, and M. Jansen, Hg₂Ru₂O₇, a new pyrochlore showing a metal-insulator transition, *J. Mater. Chem.* **17**, 1356 (2007).
- [54] J. van Duijn, R. Ruiz-Bustos, and A. Daoud-Aladine, Kagome-like lattice distortion in the pyrochlore material Hg₂Ru₂O₇, *Phys. Rev. B* **86**, 214111 (2012).
- [55] M. F. Mostafa, A. Hassen, and H. P. Kunkel, Irreversibility line of an Ag-doped Hg-based superconductor, *Supercond. Sci. Technol.* **23**, 085010 (2010).
- [56] N. Sakamoto, T. Akune, and U. Ruppert, AC susceptibility studies of inter-grains in Hg-1223 superconductors, *J. Phys.: Conf. Ser.* **97**, 012067 (2008).
- [57] M. Kubo, T. Akune, N. Sakamoto, H. R. Khan, and K. Lüders, Superconductivity of Ag-added composites of Hg-1223 grained Bean model, *Physica C* **463-465**, 478 (2007).
- [58] C. A. Passos, M. T. Orlando, F. D. Oliveira, P. C. Da Cruz, J. L. Passamai, C. G. Orlando, N. A. Elói, H. P. Correa, and L. G. Martinez, Effects of oxygen content on the properties of the Hg_{0.82}Re_{0.18}Ba₂Ca₂Cu₃O_{8+d} superconductor, *Supercond. Sci. Technol.* **15**, 1177 (2002).
- [59] K. Knížek, M. Veverka, E. Hadová, J. Hejtmánek, D. Sedmidubský, and E. Pollert, Synthesis of HgBa₂CuO_{4+δ} by sol-gel method under controlled oxygen pressure; Electron and thermal transport properties, *Physica C: Superconductivity* **302**, 290 (1998).
- [60] Y. Yu, Z. Y. Zeng, X. N. Xu, H. M. Shao, M. J. Qin, X. Jin, X. X. Yao, X. S. Rong, B. Ying, and Z. X. Zhao, Temperature dependence of the critical current determined from magnetic relaxation in HgBa₂Ca₂Cu₃O_{8+δ}, *Physica C: Superconductivity* **298**, 240 (1998).
- [61] J. Karpinski, H. Schwer, I. Mangelschots, K. Conder, A. Morawski, T. Lada, and A. Paszewin, Crystals of Hg superconductors, *Nature (London)* **371**, 661 (1994).
- [62] H. Schwer, J. Karpinski, K. Conder, L. Lesne, C. Rossel, A. Morawski, T. Lada, and A. Paszewin, X-ray single-crystal structure refinement of the 129 K superconductor Hg_xPb_{1-x}Ba₂Ca₃Cu₄O_{10+δ}, *Physica C: Superconductivity* **243**, 10 (1995).
- [63] C. T. Lin, Y. Yan, K. Peters, E. Schönherr, and M. Cardona, Flux growth of Hg_{1-x}Re_xBa₂Ca_{n-1}Cu_nO_{2n+2+δ} single crystals by self-atmosphere, *Physica C: Superconductivity* **300**, 141 (1998).
- [64] R. Gatt, E. Olsson, A. Morawski, T. Lada, A. Paszewin, I. Bryntse, A. M. Grishin, Y. Eeltsev, P. Berastegui, and L. G. Johansson, Hg-1212 and Hg-1223 single crystals: Synthesis and characterisation, *Physica C: Superconductivity* **276**, 270 (1997).
- [65] J. Karpinski, 20 years high pressure materials synthesis group activity after discovery of high-T_c superconductors, in *High T_c Superconductors and Related Transition Metal Oxides*, edited by A. Bussmann-Holder and H. Keller (Springer-Verlag, Berlin, Heidelberg, 2007), pp. 167–175.
- [66] J. Karpinski, High pressure in the synthesis and crystal growth of superconductors and IIIN semiconductors, *Philos. Mag.* **92**, 2662 (2012).
- [67] E. Biehl and H. J. Deiseroth, Rb₅Hg₁₉: Eine neue, geordnete defektvariante des BaAl₄-strukturtyps, *Z. Anorg. Allg. Chem.* **625**, 389 (1999).
- [68] A. Extremera, On the surface magnetization in superconducting NaHg₄, *J. Less-Common Met.* **134**, 195 (1987).
- [69] A. Extremera, The magnetic behaviour of NaHg₄ peritectic, *Phys. Status Solidi A* **105**, 281 (1988).
- [70] A. Extremera, Excess molar volume and m/m* effects in the magnetic behaviour of liquid HgNa alloys, *J. Phys.: Condens. Matter* **3**, 3663 (1991).
- [71] C. Stock, J. A. Rodriguez-Rivera, K. Schmalzl, F. Demmel, D. K. Singh, F. Ronning, J. D. Thompson, and E. D. Bauer, From Ising Resonant Fluctuations to Static Uniaxial Order in Antiferromagnetic and Weakly Superconducting CeCo(In_{1-x}Hg_x)₅ (x = 0.01), *Phys. Rev. Lett.* **121**, 037003 (2018).
- [72] W. Bao, Y. C. Gasparovic, J. W. Lynn, F. Ronning, E. D. Bauer, J. D. Thompson, and Z. Fisk, Commensurate magnetic structure of CeRhIn_{4.85}Hg_{0.15}, *Phys. Rev. B* **79**, 092415 (2009).
- [73] J. Tang Jr. and K. A. Gschneidner, Antiferromagnetic ordering in CeHg₃, *Phys. B: Condens. Matter* **230-232**, 186 (1997).
- [74] G. Bruzzone and F. Merlo, The lanthanum-mercury system, *J. Less-Common Met.* **44**, 259 (1976).
- [75] H. H. Hill, Early Actinides: The Periodic System's f Electron Transition Metal Series, *Nucl. Met., Met. Soc. AIME* **17**, 2 (1970).
- [76] A. Misiuk, J. Mulak, A. Czopnik, and W. Trzebiatowski, Magnetic properties of some uranium compounds of the AlB₂ type, *Bull. Acad. Pol. Sci.* **20**, 337 (1972).

- [77] V. Sechovsky and L. Havela, *Intermetallic Compounds of Actinides*, Handbook of Ferromagnetic Materials, Vol. 4 (Elsevier Science, Amsterdam, 1988), pp. 309–491.
- [78] Z. Fisk, H. R. Ott, and J. L. Smith, Chemical physics of heavy electron uranium compounds, *J. Less-Common Met.* **133**, 99 (1987).